12th Brazilian Congress of Manufacturing Engineering
May 10th-12th, 2023, Brasilia, DF, Brazil

DIRECTED ENERGY DEPOSITION OF H13 TOOL STEEL FOR MOLD AND DIE REPAIR

Alcindo Fernando Moreira
University of Sao Paulo, Sao Carlos School of Engineering, Department of Production Engineering, Sao Carlos – SP, Brazil
alcindo@usp.br

Fabio Edson Mariani
University of Sao Paulo, Sao Carlos School of Engineering, Department of Production Engineering, Sao Carlos – SP, Brazil
mariani-fabio@usp.br

Reginaldo Teixeira Coelho
University of Sao Paulo, Sao Carlos School of Engineering, Department of Production Engineering, Sao Carlos – SP, Brazil
rtcoelho@sc.usp.br

Wayne Nguyen Hung
Texas A&M University, Engineering Technology & Industrial Distribution Department, College Station, Texas, USA
hung@tamu.edu

Abstract. *The Directed Energy Deposition (DED) process can be used for engineering component repair. This paper presents a preliminary research study of repairing an injection mold by utilizing DED as an effective metal additive manufacturing. Factorial engineering experiments were designed to optimize the microstructure of DED deposited H13 powder on rolled plates of the same material. The DED deposition at 56 J/mm^2 energy density, 6.50 mg/mm^2 powder density, 67° scanning strategy at 0.9 mm hatching distance provided the optimal microstructure with minimum porosity. Fast cooling rate of a deposited layer resulted in significant higher hardness level due to the inevitable martensitic transformation of a thin deposited layer on a large substrate. Despite isolated pores, shear testing confirmed that the high-quality interface was achieved since cracks initiated and propagated outside of the heat affected zone and away from the interface.*

Keywords: *H13 tool steel; Directed energy deposition; Interface; Shear testing.*

1. INTRODUCTION

Tool steels and superalloys are special group of engineering materials that possess exceptional mechanical properties or chemical resistance at high operating temperature. They are typically used for high demanding applications in oil/gas, aerospace, nuclear, turbomachinery, manufacturing industries as tooling in high temperature manufacturing processes or components in actual operation conditions. The explosion of metal additive manufacturing (MAM) innovation has led to revolutionary fabrication methods of engineering components. Among available MAM techniques such as directed energy deposition (DED), powder bed fusion (PBF), binder jetting, wire-arc additive manufacturing (WAAM), and cold spray additive manufacturing. Although the DED is inferior to PBF process when comparing surface finish and accuracy, but the DED's advantages include fast-depositing rate, suitable economy range, and suitability for repair of engineering components like high temperature mold and die where H13 tool steel is typically utilized. Technical issues related to DED must be addressed to assure long term reliability of a repaired component. Fabrication by fusing layers of melted powders would introduce point, line, and volume defects in the part. Porosity, solidification shrinkage, microcracks, harmful residual stress, anisotropy, rough surface finish, distortion, undesirable micro structure, insufficient bonding of deposited materials on a substrate… are among key issues with MAM. The objectives of this research were to:

i) Optimize DED process parameters for depositing of H13 tool steel on the same substrate, and
ii) Evaluate the strength and integrity of the interface between DED'ed and wrought substrate.

2. LITERATURE REVIEW

The H13 tool steel, capable of maintaining its mechanical properties up to 540 C, is commonly used as die or mold for hot work applications like injection molding, die casting, hot extrusion, or hot forging. The nominal chemical compositions of H13 include Fe as the major element alloying with 0.37wt% C, 1.1 Si, 0.39 Mn, 4.7 Cr, 1.27 Mo, 0.97 V, and 0.04 W [Abdel-Latif et al., 2021]. These authors studied the effects of PBF parameters on properties of printed H13. A slow scanning speed of 150 mm/s and volume energy of 95 J/mm^3 produced the best materials with highest hardness (50 HRC), highest impact toughness (10 J), highest tensile strength (1400 MPa), and highest yield strength (1200 MPa), while achieving the longest ductility (7%). These properties were due to finer porosity in more retained austenite and the least amount of martensite.

Porosity is always an issue with MAM. Pinkerton et al. (2008) attempted to repair H13 components by DED depositing on rectangular and triangular slots. Although the slots were filled completely, the porosity at the interface between the original and DED layer was a problem. One technique to reduce porosity was to rescan a previously deposited layer to remelt and redistribute/eliminate pores. By first scanning H13 in a PBF system at 600 mm/s then rescanning at 400 mm/s, Jung et al. (2019) reported that their samples had reduced porosity and achieved a high density of 99.94% and 53.5 HRC hardness.

Although having the same compositions and elements, the microstructure of wrought materials fabricated by traditional techniques like casting, hot rolling, or hot forging is different from that of additively manufactured materials. The H13 steel powder in MAM process quickly raises to temperature exceeding its melting temperatures due to rapid heating by either a powerful laser or an electron beam. The molten pools cooled down quickly due to their small sizes when surrounding by a massive metallic block in cool and blowing inert gas atmosphere, the quenching-like action promotes very fast cooling rate and transforms austenitic structure into the hard and brittle martensite. Therefore, the hardness and strength of H13 fabricated by MAM route are expected to be very high.

The application of MAM for repairing metal components has been studied by many researchers. Saboori et al. (2019) compared different repairing techniques by welding (electron beam welding, tungsten inert gas welding, plasma transferred arc welding), high velocity oxyfuel thermal spray, electro spark, and DED. Successful repair of Inconel 625, cast iron, and Ti 6Al 4V was reported but the repair of H13 steel using DED method was flagged with serious porosity problem. The same conclusion was made by Pinkerton et al. (2008). In addition to reparation, the DED can be used to build multi-material structures, coating/cladding on metallic substrate, alloying design, and fabricating functionally gradient structures (Svetlizky et al., 2021). Feeding metallic powder to a DED laser head was preferred over wire-feeding since the former approach can result in better dimensional accuracy, finer surface finish on complex geometry components. The authors recommended combining the hybrid DED additive process with a subtractive process such as multi-axis CNC milling to enhance the part quality, accuracy and finish. A hybrid system to include both additive and subtractive, however, has posed technical challenges for programming, controlling of contamination among chips and virgin powder, contamination issues when using cutting fluid during machining… A different hybrid system including directed energy arc deposition and in-situ hot rolling was performed by Xu et al. (2023). These researchers combined WAAM using a tungsten inert gas (TIG) welding torch gun and a roller to deposit 316L stainless steel on a cylindrical shaft of the same material. Fine grains were observed in the WAAM deposited zone, but columnar grains growing perpendicular to the interface were observed. The hot rolling process, performed immediately after each laser deposed bead, would close most internal pores and improved the part quality. The hardness level increased from 180 to 250 VHN from substrate toward the deposited layer; all the yield strength, tensile strength, and elongation increased compared to those at the base material due to grain boundary strengthening mechanism of the fine-grain structure. Ackermann et al., (2018) evaluated the effects of L-PBF parameters on mechanical properties of H13 tool steel. Tensile, hardness, and impact specimens were fabricated in the as-printed, annealed, quenched & tempered to compare against properties of the wrought specimens. High level of martensite in the as-printed H13 contributed to high tensile strength but low ductility. After tempering, the strength and ductility data then approached those of wrought material. Similar trends were experimentally found for the hardness and impact data.

Table 1 summarizes the strength and hardness of H13 fabricated by either L-PBF or DED methods. Table 2 tabulates the reported strength and estimated hardness of wrought H13 steel using online conversion table for steel [Carbide Depot, 2023]

Table 1. Strength and hardness of H13 tool steel by MAM route.

Additive process	Parameter	Heat treatment	Tensile strength (MPa)	Hardness	Source
L-PBF	Volume energy 47.6-100 J/mm^3	None	1620-1920	600 VHN (55 HRC)	Huang et al., 2022
L-PBF	Double scan at 600 mm/s then 400 mm/s	None		570 VHN (53.5 HRC)	Jung et al., 2019
L-PBF	90 W, scan at 200 mm/s	None		600 VHN (55 HRC)	Lee et al., 2019
L-PBF	350W, scan at 1400mm/s	Anneal	1855	673 VHN (59 HRC)	Ackermann et al., 2018
L-PBF	350W, scan at 1400 mm/s	Quench & temper	1313	412 VHN (42 HRC)	Ackermann et al., 2018
DED	2 kW, scan at 330 cm/min	None	1820	700 Knoop (58.5 HRC)	Mazumder et al., 1997
DED	Area energy 40 J/mm^2	None		613 VHN (56 HRC)	Park et al., 2016

Table 2. Mechanical properties of wrought and cast H13 tool steel

Type	Heat-treatment	Yield strength (MPa)	Tensile strength (MPa)	Estimated hardness (*)	Source
Cast	Annealed	370	670	206 VHN (12 HRC)	Xue et al., 2018
Wrought	Annealed	510	676	208 VHN (13 HRC)	Xue et al., 2018
Wrought	1010°C quench, 605°C temper	1290	1495	471 VHN (47 HRC)	Xue et al., 2018
Wrought	1010°C quench, 527°C temper	1570	1960	613 VHN (56 HRC)	Xue et al., 2018
Wrought	Air quench, double temper 600°C, 2 hours	1230	1393	440 VHN (45 HRC)	Ackermann et al., 2018
Wrought	Air /oil quench from 995-1025°C		1990	595 VHN (55 HRC)	Matweb.com
Wrought	Quench, temper	1000-1380	1200-1590	375-506 VHN (38-49 HRC)	Azom.com

* Carbide Depot, http://www.carbidedepot.com/formulas-hardness.htm

3. EXPERIMENTS

The ROMI DED system was utilized for depositing blocks on H13 powder on annealed H13 tool steel plate. Previous studies suggested the optimal DED parameters to be 750-watt laser with ϕ2 mm spot size; the Argon gas flow was kept constant at 4 L/min through the nozzle, 5 L/min for the carrier, and 10 L/min for shielding. The H13 powder flow rate was 5.2 g/min using powder in the range of 45-106 µm. Other parameters included:

- Scanning angles: alternate 0/90° layers and 67° rotation of successive layers (Fig. 1)
- Laser scanning speed: 400 and 600 mm/min
- Stepover: 45% and 55% to form either 0.9 or 1.2 mm hatching distances respectively for a 2 mm wide bead (Fig. 2)

The combined and governing DED parameters are:

$$E_{area} = \frac{P}{Vd} \quad (1)$$

$$E_{linear} = \frac{P}{V} \quad (2)$$

$$F = \frac{G}{Vd} \quad (3)$$

Where E_{area}: area energy density (J/mm^2)
E_{linear}: linear energy density (J/mm)
F: powder density (g/mm^2)
P: laser power (W)
V: laser scanning speed (mm/s)

d: laser beam size (mm)

The area energy density in this experiment varied from 37 to 56 J/mm^2 while the linear energy density varied from 75 to 112 J/mm, and those for powder density were 4.33 to 6.50 mg/mm^2 for high and low scanning speed respectively.

A total of 9 blocks (17x22 mm and 10 mm high) were deposited on a rolled H13 plate (132 x132 mm x 32 mm high). The alternate positions of successive deposited blocks were chosen to minimize conductive heating effect on adjacent blocks (Fig. 3). Each block was numbered according to respective scanning parameters (Table 3). Two replicates were fabricated for repeatability.

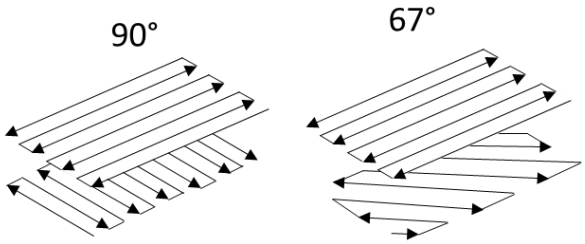

Figure 1 – Two scanning strategies with alternate 0/90° and 67° scanning direction

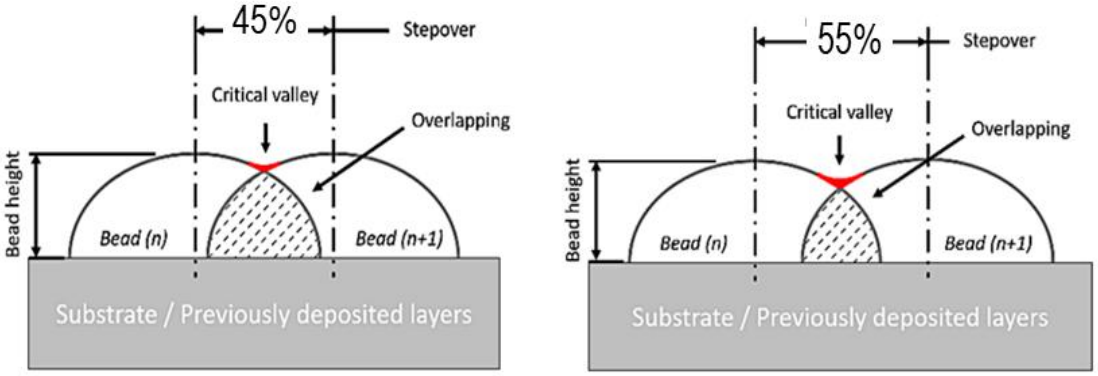

Figure 2 – Two stepover strategies 45% (0.9mm hatch) and 55% (1.1mm hatch) for 2 mm wide bead

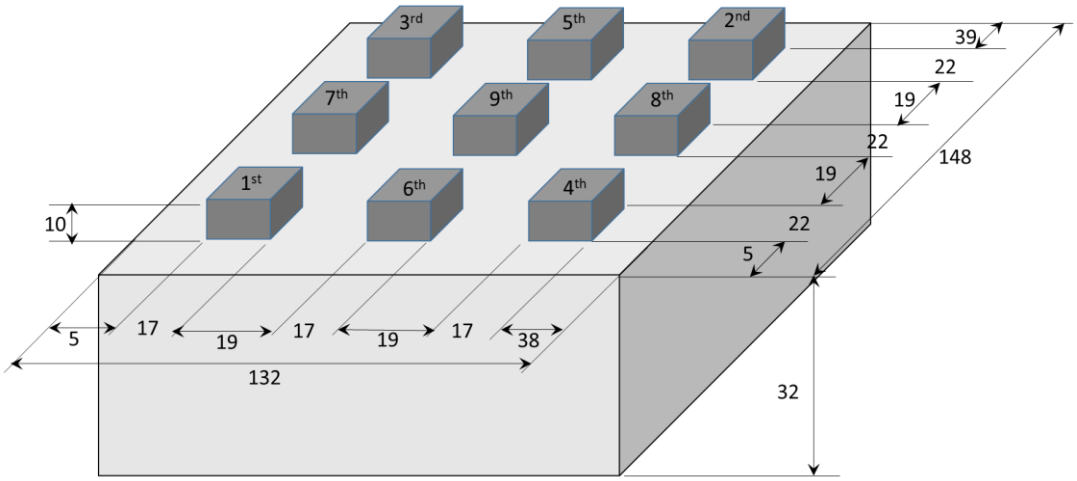

Figure 3 – Layout of deposited blocks on wrought substrate. Unit: mm

Table 3. Scanning parameters

Block #	Scanning angle (°)	Stepover (%)	Hatch distance (mm)	Scanning speed (mm/min)
1	0 / 90	45	0.9	400
2	0 / 90	45	0.9	600
3	0 / 90	55	1.1	400
4	0 / 90	55	1.1	600
5	67	45	0.9	400
6	67	45	0.9	600
7	67	55	1.1	400
8	67	55	1.1	600
9*	67	45	0.9	600

* This block was deposited with 10% power decrement for each successive layer.

After DED, the plates were subjected to different heat treatment and then cut by wire-type electrical discharged machining to fabricate different specimens for microstructure study and shear test (Fig. 4).

- Stress relieving. A plate was stress relieved by heating to 650 °C for 2 hours, furnace cooling to 500 °C then air cooling to room temperature. All samples were stress-relieved before being sectioned and analyzed due to possible high residual stress in deposited plates.
- Hardening. A plate was heated to 1030 °C for 4 hours, oil quenched, then tempered twice at 575 °C for 2 hours following by air cooling to room temperature.
- Microstructure study. The specimens were hand ground and polished in slurry of 1 µm then 0.5 µm alumina particles. They were etched in Nital etchant (5% HNO_3 + 95% CH_3OH), rinsed in water, isopropyl alcohol and blew dried with hot air to reveal the microstructure. The material hardness across depositing interface was measured with the Buehler 1600-6300 microhardness tester setting at 200gf load and 15s dwelling time.
- Shear testing. The stress-relieved DED specimens were polished on one side and then etched in Nital solution to reveal the depositing interface. A shearing tool, positioned closed to the interface, compressed and sheared the sample on the Instron 2382 universal tester at 3 mm/min travel rate. A test was stop when the system detected a sudden drop of the shearing force (Fig. 5).
- Fracture study. The sheared pairs were washed in acetone, then hot molded in Bakelite with the Arotec Pre 30Mi system. They were hand ground and finished polishing with 0.5 µm alumina slurry, etched in Nital etching solution to reveal the microstructure and fracture surface. Microhardness was performed again across the interface of sheared specimens.

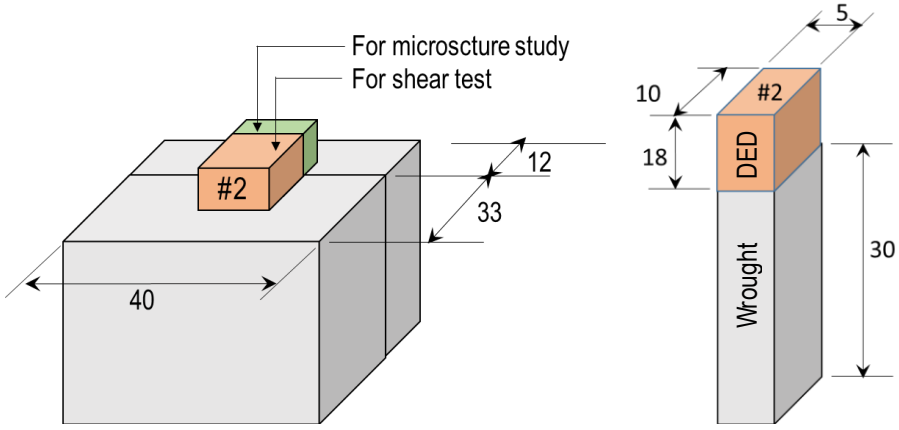

Figure 4 – Wire EDM sectioning (left) and shear test specimen (right). Unit: mm

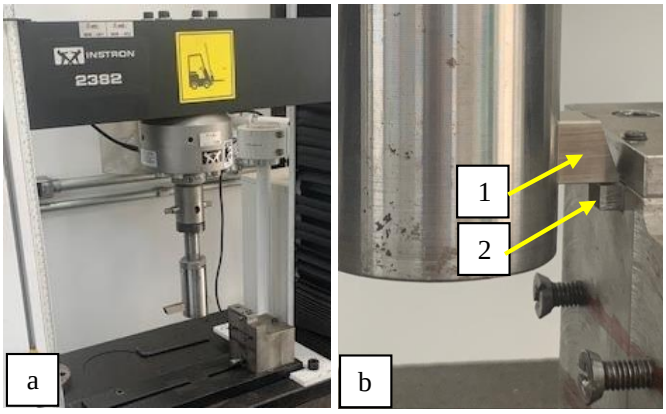

Figure 5 – (a) Set up for shearing test per DIN EN-15340 on the Instron tester, and (b) Close up of the shearing tool "1" and workpiece "2"

4. RESULTS AND DISCUSSION

Microhardness across the interface of DED and wrought materials are plotted in Fig. 6. There was no significant hardness difference on these specimens due to difference scanning strategies. The H13 steel, deposited on a large cold substrate, was practically quenched in argon gas at high cooling rate to form martensite as shown by the very high hardness of 600 Vickers hardness (55 HRC). Such high hardness of the DED layer, approximately 3 times harder compared to that of the annealed wrought H13 substrate, would cause significant residual strain at the interface and distort a thin substrate. Although stress-relived, the high hardness would pose a challenge in post processing. The same level of hardness (about 600 VHN) was also achieved in another experimental study when printing H13 with L-PBF in the energy range of 47.6-100 J/mm^3 (Table 1).

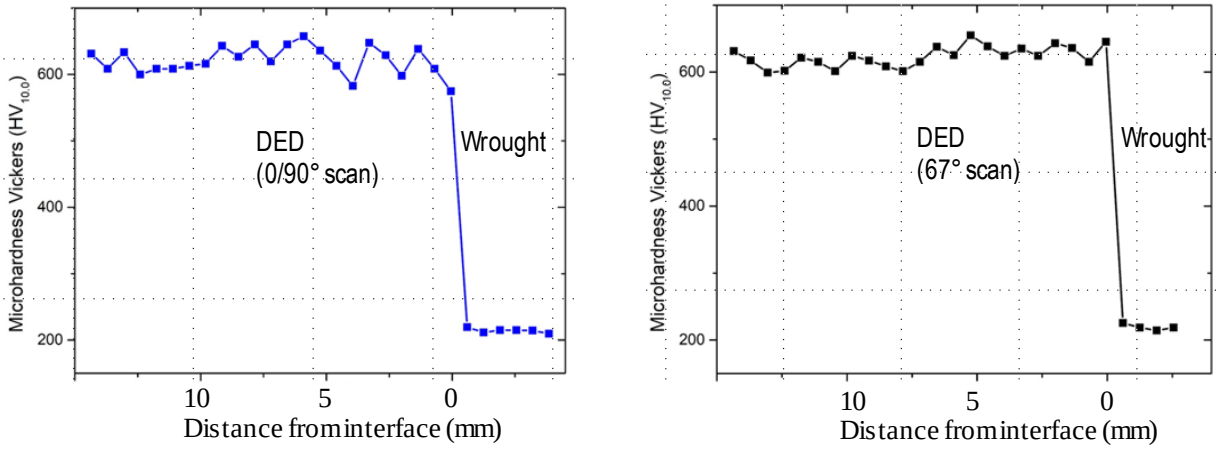

Figure 6 – Microhardness across the interface for samples with different scanning strategies.

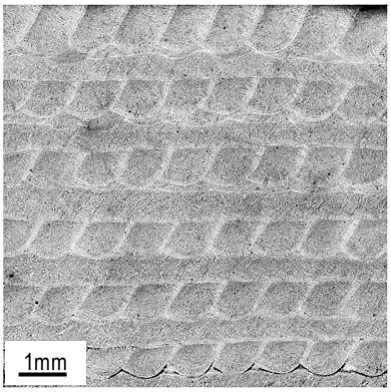

Figure 7a – Microstructure of specimen #5 (37 J/mm^2, 4.33 mg/mm^2, 0/90° scan, 0.9 mm hatch)

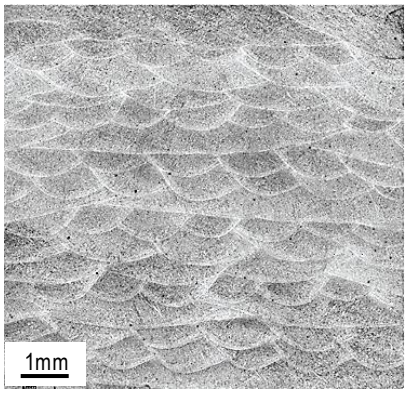

Figure 7b – Microstructure of specimen #7 (37 J/mm^2, 4.33 mg/mm^2, 67° scan, 0.9 mm hatch)

Typical microstructure of 0/90° and 67° scanned specimens are shown in Fig. 7. The former produced more spherical pores when observed under an optical microscope. The optimal parameters for least porosity were experimentally found to be 56 J/mm^2 area energy density, 6.50mg/mm^2 powder density when scanning with 67° scanning strategy.

Three shear samples (specimens #18, 19, and 20) were DED printed at optimal conditions, stress relieved, wire EDM cut, slightly etched to show the interfaces, before subjected to shear testing. Figure 8 and Table 4 summarize the shear test results. The specimen 18 was completely sheared into two pieces, but the others were partially sheared after stopping of the shearing action.

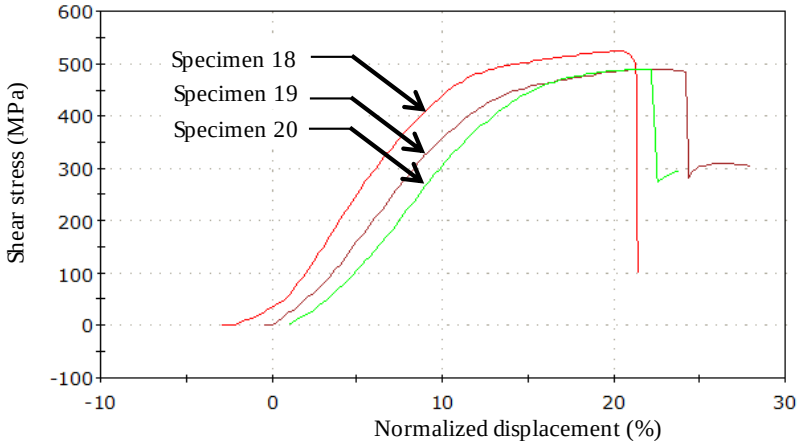

Figure 8 – Shear test results. The specimen 18 was completely sheared of, while the others were partially sheared.

Table 4. Summary of shear test results

Specimen #	Shear stress at yield (MPa)	Maximum shear stress (MPa)
18	414.5	523.3
19	398.9	490.3
20	420.0	489.9
Average	411.1	501.0
Standard deviation	10.95	19.29

Microstructure of the sheared specimens are shown in Fig. 9. Typical molten and solidified metal pools at corresponding hatching distance are visible. The shearing planes for all three specimens were in the wrought material, away from the interface and slightly outside of the heat affected zone (HAZ). Figures 10a and 10b show keyhole pores at the interfaces; a larger pore with an un-melted powder particle is seen in Figure 10c. Since cracks were in the wrought material and not at the interface, the bonding strength along interface must be very strong except at the pores.

The selected parameters (5.2 g/min powder feeding rate, 750 W laser power, 400-600 mm/min laser feeding rate) resulted in 75-112 J/mm linear energy density according to equation (2). Such selection was slightly higher than those from other study for H13 [Svetlizky et al., 2021]; however, the parameters in this study provided minimum porosity and strong interfacial bonding as seen after sectioning (Figs. 10-11).

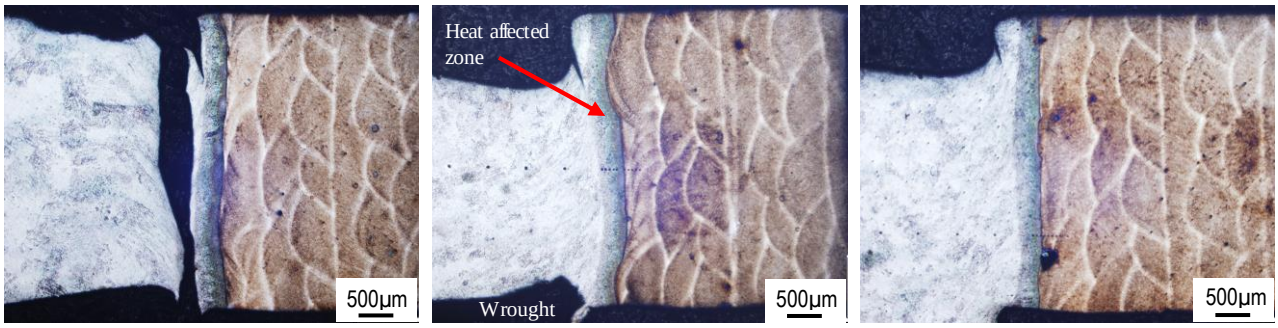

Figure 9 – Shearing of DED/wrought interface for specimens #18, #19, and #20 (left to right).
All samples were prepared at 37 J/mm^2, 4.33 mg/mm^2, 67° scan, 0.9 mm hatch

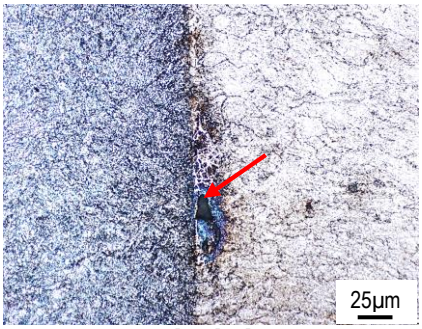

Figure 10a – A keyhole at wrought/DED interface. Specimen #18.

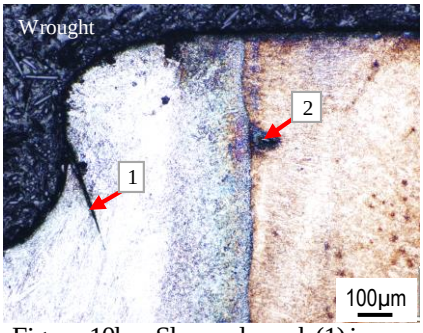

Figure 10b – Sheared crack (1) in wrought region and keyhole (2) in DED region. Specimen #20.

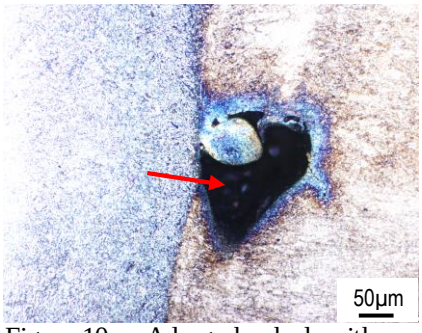

Figure 10c – A large keyhole with un-melted powder particle at wrought /DED interface. Specimen #20.

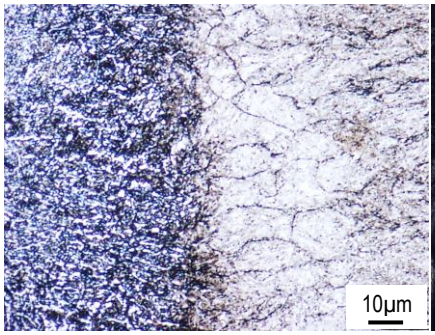

Figure 11a – Columnar grains of DED deposited material at the interface. Specimen #18.

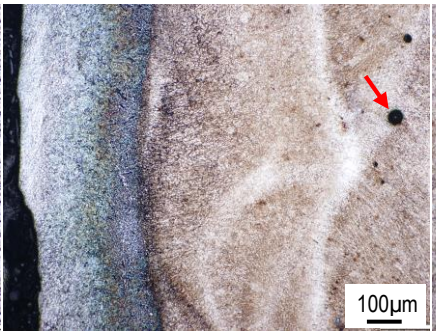

Figure 11b – Spherical pores between DED layers but not at the interface. Specimen #18.

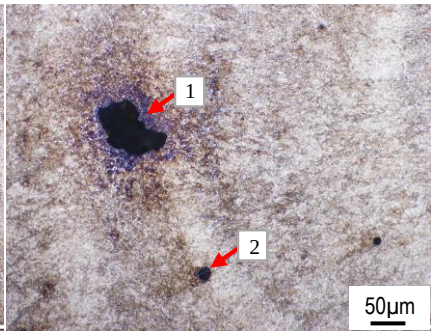

Figure 11c – A rare keyhole (1) and random smaller spherical pores (2) in DED material. Specimen #19.

Figure 11a shows the interface at high magnification. Columnar direction of the DED'ed grains indicates the heat transfer from the molten DED grains toward the large and cooler substrate. The thin substrate surface is first heated above its melting temperature (approximately 1427 °C), melts and welds to the first DED layer. Upon fast cooling, the austenite layer in the HAZ of wrought material transforms into martensite. Subsequent depositing of DED layers provides thermal energy to the HAZ and tempers the martensitic layer, therefore, transforming the HAZ into a strong and tough layer that effectively resists the shear stress. As the result, a crack would initiate just outside of the HAZ of the wrought material.

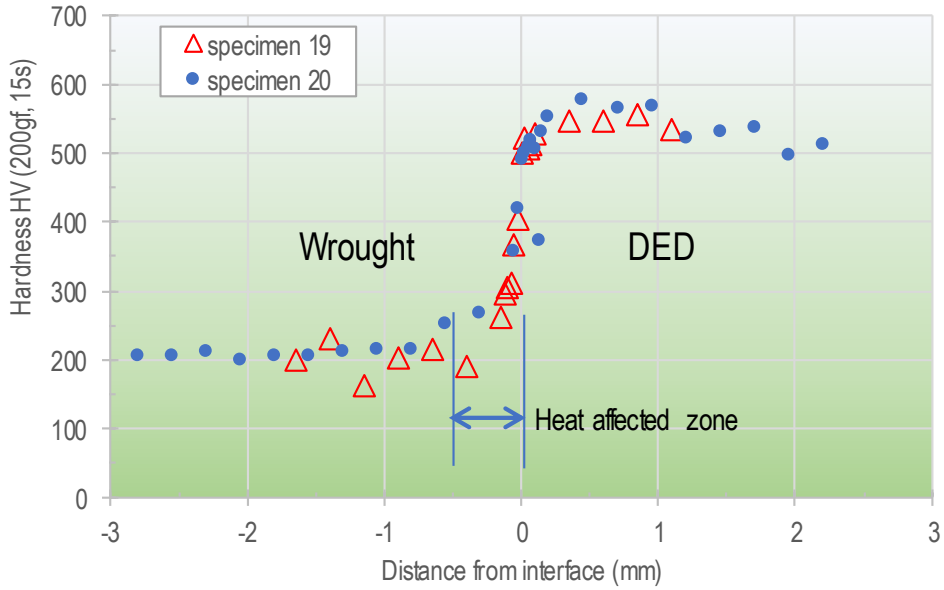

Figure 12 – Microhardness across the deposited interface.

Published literature usually reports either hardness or tensile properties rather than shear properties. Considering a case of pure shear, the yield strength predicted by the distortion-energy theory is given by [Juvinall, 1967]:

$$Shear\ strenght \approx 0.577 \times Tensile\ strength \quad (4)$$

The average of measured shear strength of the H13 DED deposited on wrought H13 is 501 MPa (Table 4); using equation (4), the calculated tensile strength of the specimen would be 868 MPa. This value is higher than tensile strength of 676 MPa for annealed wrought H13 but less than 1200-1990 MPa of the quenched and tempered material (Table 2). This suggests that the wrought material near the interface was transformed partially to martensite due to rapid heating and cooling in the HAF. A slight increase of hardness of wrought material within 0.45 mm zone from the interface is shown in Fig. 12. This 0.45mm-zone is approximately the same width of HAZs of three specimens in Fig. 9.

5. SUMMARY AND FUTURE WORK

Simulation of mold repair was performed by directed energy depositing (DED) of H13 tool steel on rolled H13 substrate. The preliminary results showed:

1) The DED deposition at 56 J/mm^2 energy density, 6.50 mg/mm^2 powder density, 67° scanning strategy at 0.9 mm hatching distance was successfully implemented to produce consistent micro structure with minimum porosity.
2) Very strong interface between DED'ed and wrought materials was achieved. Cracks initiated and propagated just outside of heat affected zone in the wrought material despite isolated keyholes or pores along the interface.
3) The deposited DED layer contained martensitic structure; its high hardness (600 VHN) was three times harder than that of the substrate (200 VHN). Post processing of the DED layer would be a challenge.
4) Additional work will be performed to study the machinability of the hardened DED deposited layers.

6. ACKNOWLEDGEMENTS

This research work is supported by the 2019 TAMU-USP FAPESP project #19/08926-6. The authors thank Material Institute of Brazil in Sao Carlos for performing the shear testing.

7. REFERENCES

Abdel-Latif M., Abdel-Ghany K., El-Mahallawy N., and Mattar T., 2021. "Effect of Laser Speed on Microstructure and Mechanical Properties of AISI H13 Tool Steel Prepared by Laser Powder Bed Fusion Process," Journal of Materials Engineering and Performance on Additive Manufacturing. Vol. 30 (12), pp. 8821–8830. "https://doi.org/10.1007/s11665-021-06321-y

Ackermann M., Šafka J., Voleský L., Bobek J., and Kondapally J.R., 2018. "Impact Testing of H13 Tool Steel Processed with Use of Selective Laser Melting Technology," Materials Science Forum, Vol. 919, pp 43-51. DOI:10.4028/www.scientific.net/MSF.919.43

Carbide Depot, Hardness conversion chart, http://www.carbidedepot.com/formulas-hardness.htm, access Jan. 2023.

Jung I.M., Choe J., Yun J., Yang S., Yang D.Y., Kim Y.J., Yu J.H., 2019. "Dual speed laser re-melting for high densification in H13 tool steel metal 3D printing," Arch. Metall. Mater. 64 (2019), 2, 571-578.

Juvinall R.C., 1967. Engineering Considerations of Stress, Strain, and Strength, McGraw-Hill, p.87.

Lee J., Choe J., Park J., Yu J.H., Kim S., Jung I.D., Sung H., 2019. "Microstructural effects on the tensile and fracture behavior of selective laser melted H13 tool steel under varying conditions," Materials Characterization 155 (2019) 109817.

Li L., Zhang Z., and Liou F., 2021. "Experimental and Numerical Investigation in Directed Energy Deposition for Component Repair," Materials, MDPI, 1409. https://doi.org/10.3390/ma14061409.

Mazumder J., Choi J., Nagarathnam K., Koch J., and Hetzner D., 1997. "The Direct Metal Deposition of H13 Tool Steel for 3-D Components," International Symposium on The Processing and Manufacture of Light Metals, Ontario, Canada.

Oh W.J., Lee W.J., Kim M.S., Jeon J.B., Shim D.S., 2019. "Repairing additive-manufactured 316L stainless steel using direct energy deposition," Optics and Laser Technology, 117, pp. 6–17.

Park J.S., Park J.H., Lee M.G., Sung J.H., Cha K.J., and Kim D.H., 2016. "Effect of Energy Input on the Characteristic of AISI H13 and D2 Tool Steels Deposited by a Directed Energy Deposition Process," Metallurgical and Materials Transections A, Vol. 47A, pp. 2529-2535. DOI: 10.1007/s11661-016-3427-5

Pinkerton A.J., Wang W., and Li L., 2008. "Component repair using laser direct metal deposition," Proceedings Institution of Mechanical Engineers, Engineering Manufacturing, Vol. 222:7, pp. 827-836. https://doi.org/10.1243/09544054JEM100

Saboori A., Aversa A., Marchese G., Biamino S., Lombardi M., and Fino P., 2019. "Application of Directed Energy Deposition-Based Additive Manufacturing in Repair," Applied Sciences, MDPI, 9, 3316. DOI:10.3390/app9163316.

Svetlizky D., Das M., Zheng B., Vyatskikh A.L., Bose S., Bandyopadhyay A., Schoenung J.M., Lavernia E.J., Eliaz N., 2021. "Directed energy deposition (DED) additive manufacturing: Physical characteristics, defects, challenges and applications," Materials Today, Vol. 49, pp. 271-295.

Xu H., Zhang Q., Tian T., Niu L., Li H., Han B., Zhu H., and Wang X., 2023. "In-situ hot rolling directed energy deposition-arc repair of shafts," Additive Manufacturing, 61-103362, https://doi.org/10.1016/j.addma.2022.103362

Xue A., 2018. "Laser Consolidation—A Rapid Manufacturing Process for Making Net-Shape Functional Components," *Advances in Laser Materials Processing: Technology, Research and Applications*, Woodhead Publishing Series, pp. 461-505, https://doi.org/10.1016/C2015-0-05718-5.

8. RESPONSIBILITY NOTICE

The authors are the only responsible for the printed material included in this paper.